CHALMERS

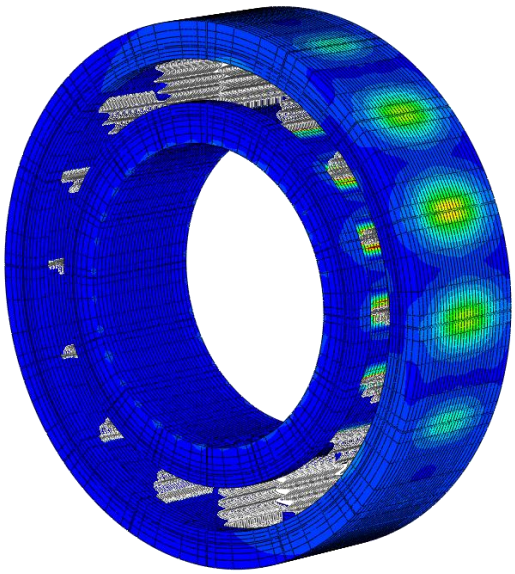

Modelling of roller bearings in ABAQUS

Master's Thesis in the Applied Mechanics

EMIL CLAESSON

Department of Applied Mechanics
Division of Material and Computational Mechanics
CHALMERS UNIVERSITY OF TECHNOLOGY
Göteborg, Sweden 2014
Master's thesis 2014:16

MASTER'S THESIS IN APPLIED MECHANICS

Modelling of roller bearings in ABAQUS

EMIL CLAESSON

Department of Applied Mechanics
Division of Material and Computational Mechanics

CHALMERS UNIVERSITY OF TECHNOLOGY
Göteborg, Sweden 2014

Modelling of roller bearings in ABAQUS

EMIL CLAESSON

Master's Thesis 2014:16
ISSN 1652-8557
Department of Applied Mechanics
Division of Material and Computational Mechanics

Chalmers University of Technology
SE-412 96 Göteborg
Sweden
Telephone: + 46 (0)31-772 1000

Cover:
Simplified cylindrical roller bearing model of type C. See Section 3.3.

Name of the printers / Department of Applied Mechanics
Göteborg, Sweden 2014

Modelling of roller bearings in ABAQUS

Master's Thesis in the *Applied Mechanics*
EMIL CLAESSON
Department of Applied Mechanics
Division of Material and Computational Mechanics

Chalmers University of Technology

ABSTRACT

A useful FE-analysis requires a good knowledge of the loads that the analysed structure is subjected to. When simulating gearboxes, bearings are key components in this aspect as they transmit forces between the components in the gearbox, e.g. gear wheels, shafts and housings.

Using full FE-models of the bearings, with solid rollers and contacts, when modelling a significant part of the gearbox with several bearings is not feasible, from the view of computational cost. Thus it is necessary to have simplified bearing models.

Three simplified FE-models for roller bearings, both cylindrical and tapered bearings, have been developed. The models have different levels of complexity and computational cost. The cylindrical models have been verified against reference results from full FE-models with satisfactory result. The models for tapered bearings are still to be verified.

Key words: roller bearings

Contents

ABSTRACT I
CONTENTS III
PREFACE V
NOTATIONS VI

1 INTRODUCTION 1
1.1 Background 1
1.2 Purpose 1
1.3 Limitations 1

2 THEORETICAL BACKGROUND 2
2.1 Kinematics of roller bearings 2
2.2 Roller-raceway contact 3
2.2.1 Ideal line contact 3
2.2.2 Load-deflection relations 5

3 SIMPLIFIED FE-MODELS 8
3.1 Model A 8
3.2 Model B 10
3.2.1 Rings 12
3.2.2 Roller-flange contact 13
3.3 Model C 14
3.4 Spring stiffness 16

4 EVALUATION OF MODELS 18
4.1 Model B 18
4.1.1 Mesh convergence 18
4.1.2 Rotation stability 19
4.2 Model C 22
4.2.1 Mesh convergence 22
4.3 Forces and moments 23
4.4 Force distribution in the surrounding structure 25

5 CONCLUSIONS AND DISCUSSION 29

6 RECOMMENDATIONS AND FUTURE WORK 30

7 REFERENCES 31

A ANALYTICAL APPROACH FOR BEARING RACE LOADS AND MOMENTS 32

A.1 Cylindrical bearing subjected to pure radial load 32

A.2 General loading of tapered and cylindrical bearings 33

A.2.1 Bearing inner race forces 33

A.2.2 Bearing inner ring moments 34

B APPENDIX VOLVO GTT 36

C APPENDIX VOLVO GTT 37

D APPENDIX VOLVO GTT 38

Preface

This is my Master's Thesis in Applied Mechanics at Chalmers University of Technology. The work has been carried out at Volvo Global Truck Technologies (Volvo GTT), Drivelines and Hybrids, during the spring of 2014. Volvo GTT is responsible for developing technologies and components for the truck brands in the Volvo Group. The group Drivelines and Hybrids is responsible for the gearbox.

I would like to express my gratitude to my supervisors at Volvo, Maria Petersson and Sven Norberg for giving me the possibility to write my thesis at Drivelines and Hybrids, and for patiently explaining the behaviour of bearings and ABAQUS scripting. I would also like to thank my examiner Magnus Ekh for his input and valuable scepticism.

Göteborg, maj 2014

Emil Claesson

Notations

C3D20	Second order, 20-node brick element
CCL12	First order, 12-node cylindrical element
CCL24R	Second order, 24-node cylindrical element with reduced integration
IR	Inner ring of the bearing
OR	Outer ring of the bearing
C	Constant factor in load-deflection relation for roller-raceway contact
D	Roller diameter
K	Load deflection factor for roller-raceway contact
Q	Load in roller element
Q_f	Flange load inner tapered bearing
Q_{fr}	Radial component of flange load in tapered bearing
Q_{fa}	Axial component of flange load in tapered bearing
Q_i	Inner race load
Q_{ia}	Axial component of inner race load in tapered bearing
Q_{ir}	Radial component of inner race load in tapered bearing
Q_o	Outer race load
Q_{oa}	Axial component of outer race load in tapered bearing
Q_{or}	Radial component of outer race load in tapered bearing
b	Semiwidth for ideal line contact
d_m	Mean raceway diameter for inner and outer ring
l	Effective length of roller (roller length minus edge radius)
z'	Distance along roller length
α	Cup angle of bearing (zero for cylindrical bearing)
α_f	Flange angle in tapered bearing
α_i	Inner raceway angle in tapered bearing
α_o	Outer raceway angle in tapered bearing
δ	Approach of two points in roller-raceway contact
ψ	Roller element position in bearing
$\sum\rho$	Curvature sum for roller-raceway contact

1 Introduction

1.1 Background

The gearbox is continuously being developed for future demands of increased loads, longer lifetime and reductions of noise and weight. To do this in an effective way it is necessary to evaluate designs virtually, e.g. with CAE methodologies such as FE-analysis.

A useful FE-analysis requires a good knowledge of the loads that the gearbox will be subjected to during operation. It is also necessary to be able to correctly model how these loads affect the structure of the gearbox. Bearings are key components in this aspect as they transmit forces between the components in the gearbox, e.g. gear wheels, shafts and housings.

Using full FE-models of the bearings with contacts and solid rollers is not feasible, from the view of computational cost, when modelling a significant part of the gearbox with several bearings. Thus it is necessary to have simplified bearing models. The demand on a bearing model varies with the position of the bearing relative the area of interest in the analysis. If the position of the bearing is not close to the area of interest it is sufficient that the bearing model acts as a pivot point and allow for the correct total force to be transmitted. This requires that the model provides the correct overall stiffness and correct forces.

When the position of the bearing is close to the area of interest, then the detailed deformation and force distribution in the bearing will affect the critical area. This yields different and significantly more complex requirements on the bearing model than for the previous case.

Having bearing models of suitable complexity that is numerically stable and thoroughly tested and verified both decreases the computational time and ensure that the results are adequate. If they can be created automatically from a limited number of parameters then also the time for setting up models of gearboxes can be decreased.

The intention with this thesis work is to develop bearing models with different degree of complexity and computational cost. This gives a possibility to choose the proper model with respect to the purpose of the analysis.

1.2 Purpose

The aim of this thesis work is to develop roller bearing models, for both cylindrical and tapered roller bearings. They should be built with ABAQUS elements and automatically created from a limited number of parameters. This should be done using a MATLAB script. The models are intended to be used in static analysis.

1.3 Limitations

The contact pressure between rollers and rings will not be regarded. No physical testing will be performed. Only the cylindrical bearing models will be calibrated.

2 Theoretical background

This chapter describes the theory needed to understand how roller bearings behave under different loading conditions. Most of the theory is based on Houpert (1997) and Harris (1991).

Houpert (1997) has derived a uniform analytical approach for calculating the bearing forces and moments for both tapered and cylindrical roller bearings (and ball bearings). Some results from this analytical approach are shown, and later compared with results from the simplified FE-models. Harris (2006) (among others) presents a more complete theory for roller bearings but a uniform approach for cylindrical and tapered bearings is missing. Since this work is focusing on the development of FE-models and the analytical solutions are used only for comparison, and to explain the bearing behaviour, Houpert's approach is more suitable. However, Harris (1991) presents an even more simplified theory for calculating forces in cylindrical bearings; this approach is presented in Appendix A together with the equilibrium equations from Houpert, and is compared to the simplified FE-models Section 4.3.

The load-deflection relation for the roller-raceway contact is also discussed. The stiffness of the rollers in the simplified FE-models is based on these analytical relations.

2.1 Kinematics of roller bearings

Houpert (1997) derives a kinematic relation between the roller-raceway deformation (normal to the outer raceway) and five race displacements, see Figure 2.1. The centre of the inner ring, point I, is displaced with respect to the centre of the outer ring, point O, Figure 2.1 b). Both translations and rotations of the inner ring are regarded.

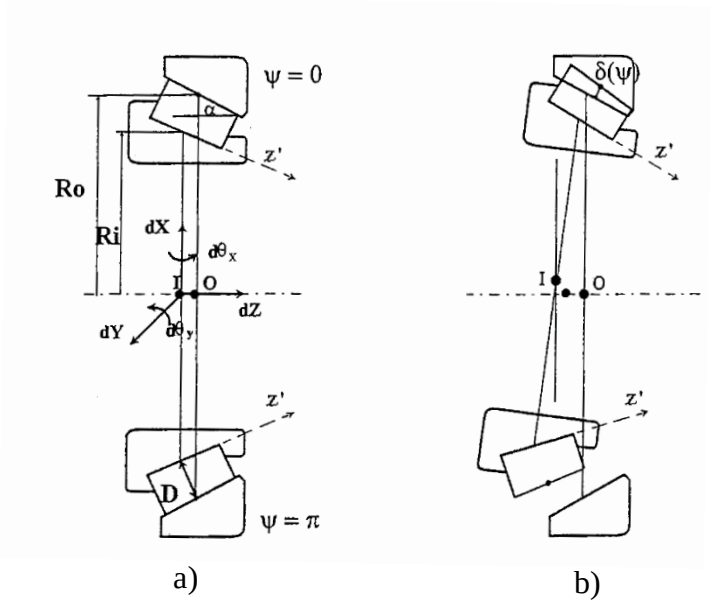

a) b)

Figure 2.1 *Displacement of the centre of the inner ring (point I) with respect to the centre of the outer ring (point O) (Houpert ,1997). a) Position of the rings when the bearing is undeformed. b) Inner ring displaced with respect to the outer ring.*

The rollers are assumed to be flat, i.e. the profile of the rollers has no crowning and the edge radius is not considered. The deformation for a roller-raceway contact is given as a function of the circumferential position of the roller in the bearing, ψ, and the distance along the roller length, z':

$$\begin{aligned}\delta(\psi, z') = &-dz\sin\alpha + \left(dx + Ri\tan\alpha\, d\theta_y\right)\cos\alpha\cos\psi \\ &+(dy - Ri\tan\alpha\, d\theta_x)\cos\alpha\sin\psi + (-d\theta_x\sin\psi + d\theta_y\cos\psi)z'\end{aligned} \tag{2.1}$$

dx and dy are the components of the radial displacement in the x- and y-direction, and dz is the displacement in the axial direction. $d\theta_x$ and $d\theta_y$ are rotations around the x-axis and y-axis, respectively. For tapered bearings the misalignment of the bearing causes an additional roller-raceway deformation at z'=0. This gives a coupling between the angular misalignment, the radial displacement, the axial displacement and the roller-raceway deformation.

For cylindrical bearings the cup angle, α, is zero. So the coupling between the misalignment of the bearing and the radial and axial stiffness for cylindrical bearings is missing in this theory.

2.2 Roller-raceway contact

The contact between the rollers and the raceways of the rings is an important aspect for determining the stiffness of bearings. The roller and raceway are initially in contact along a line, this contributes to the stiffness of roller bearings being non-linear.

2.2.1 Ideal line contact

When two cylindrical bodies with parallel axes that are in contact along a line is subjected to loading, a small contact area is formed, see Figure 2.2. The most commonly used approximation for determining the stress distribution and the width of the contact area is based on Hertzian contact theory. The following assumptions are made, cf. Harris (1991):

1. All deformations occurs in the elastic range
2. Loading is perpendicular to the surface, i.e. the effect of surface shear stresses is neglected
3. The contact area dimensions are small compared with the radii of curvature of the contacting bodies.

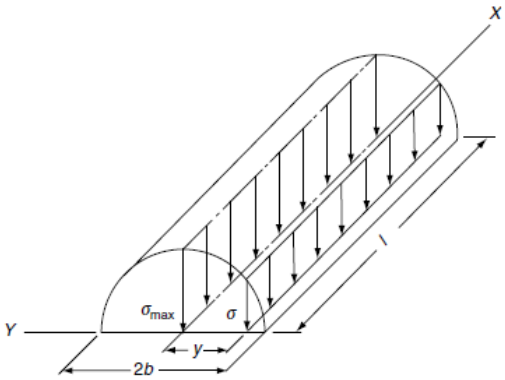

Figure 2.2 *Stress distribution and contact area for an ideal line contact based on Hertzian contact theory (Harris, 2006).*

If the bodies in contact have the same length, the stress distribution is given by:

$$\sigma = \frac{2Q}{\pi l b}\left[1 - \left(\frac{y}{b}\right)^2\right]^{1/2} \tag{2.2}$$

where Q is the roller load. Furthermore, the contact dimensions l, b and the coordinate y are introduced in Figure 2.2. Harris (1991) also gives the following approximation for the semiwidth of the contact area for steel roller bearings:

$$b = 3.35 \cdot 10^{-3}\left(\frac{q}{\sum\rho}\right)^{1/2} \tag{2.3}$$

where q is the roller load per length:

$$q = \frac{Q}{l} \tag{2.4}$$

where l is the roller effective length. The curvature sums for the inner and outer roller-raceway contact are:

$$\sum\rho_i = \frac{1}{D}\left(\frac{2}{1 - D/d_m}\right) \tag{2.5}$$

$$\sum\rho_o = \frac{1}{D}\left(\frac{2}{1 + D/d_m}\right) \tag{2.6}$$

where D is the roller diameter and d_m the mean raceway diameter for the inner and outer ring. Figure 2.3 shows the width of the contact for the inner and outer ring versus roller load.

A condition for ideal line contact is that the lengths of the bodies in contact are the same. In roller bearings the bodies in contact have different lengths and the rollers are crowded. This will lead to a somewhat different stress distribution than for ideal line contact. Stress concentrations occur at the roller ends, both in the roller and raceway,

due to the abrupt geometry change. The calculated contact width should only be seen as an approximation of the real contact. The contact width is used as a guideline when modelling the roller-raceway contact in the simplified FE-model of type C, see Section 3.3.

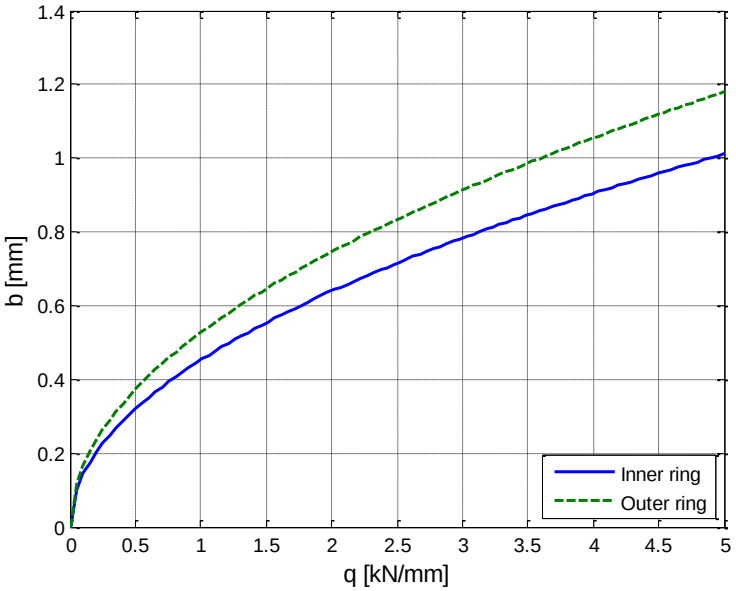

Figure 2.3 *Width of the contact area between roller and raceway, b, versus roller force, q (computed from equation (2.3))*

2.2.2 Load-deflection relations

The relation between force and deformation in a roller-raceway contact is non-linear due to the line contact, and its force dependent contact area, between the roller and raceway. Expressions for calculating the change in distance, δ, between a point in the roller and the corresponding point in the ring have been suggested by several authors, most of them are based on experiments, Harris (1991).

For a single roller-raceway contact the load-deflection relation may be expressed as, Harris (1991):

$$Q = K\delta^n \tag{2.7}$$

where Q is the roller load, K is the load-deflection factor and n is an exponent close to 1.1 for roller bearings. The total displacement of the inner ring with respect to the outer ring in the normal direction of the raceways becomes:

$$\delta_{tot} = \delta_i + \delta_o \tag{2.8}$$

and the force Q_{tot} is (due to equilibrium) equal in the inner and outer ring:

$$Q_{tot} = Q_i = Q_o \tag{2.9}$$

Hence, for one roller in contact with inner and outer ring:

$$Q_{tot} = K_n \delta_{tot}^n \tag{2.10}$$

where:

$$K_n = \left[\frac{1}{\left(1/K_i\right)^{1/n} + \left(1/K_o\right)^{1/n}} \right]^n \tag{2.11}$$

In this expression K_i and K_o refer to the load-deflection factors of the inner and outer ring, respectively. The load deflection factor is dependent on the effective length of the roller, L. Also effects from the roller diameter, D, may be included. The expression for the total roller-raceway deformation may be written in the general form:

$$Q_{tot} = C \left(\frac{L}{L_0}\right)^{n_1} \left(\frac{D}{D_0}\right)^{n_2} \left(\frac{\delta_{tot}}{\delta_0}\right)^{n_3} \tag{2.12}$$

Variables with subscript zero are used to normalize the parameters and are equal to unity when the parameters are given in millimetres. Numerical values for the constants have been given by several authors and can be seen in Table 2.1. Note that all authors include the roller effective length in the load-deflection factor, but only Houpert includes the effect from the diameter of the roller. However, he does not motivate why or whether the constants are theoretical or obtained from experiments. The influence from the diameter is however small since the exponents, n_2, is close to zero. The constants proposed by the other authors are based on experiments. Figure 2.4 shows the relation between δ_{tot} and Q_{tot} for a roller with the effective length 14.9 mm and the diameter 10.75 mm.

Table 2.1 *Constants for the load-deflection relations for roller-raceway contacts.*

Reference	C [N]	n_1 [-]	n_2 [-]	n_3 [-]
Palmgren (1959)	$3.73 \cdot 10^4$	8/9	0	10/9
Brändlein et al. (1999)	$2.65 \cdot 10^4$	0.9189	0	1.0811
Houpert (1997)	$1.67 \cdot 10^4$	0.991	0.1034	1.1

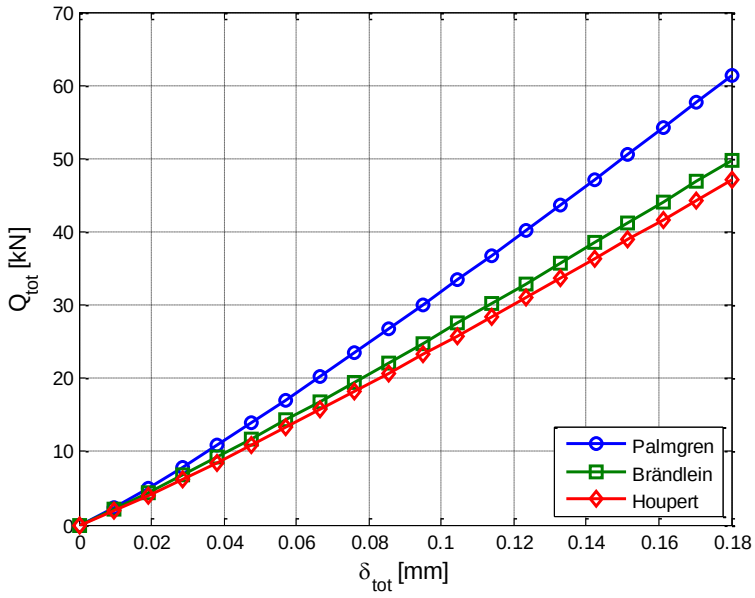

Figure 2.4 *Load Q_{tot} versus deflection δ_{tot} for contact between roller and raceways. Computed from equation (2.12) with constants according to Table 2.1.*

3 Simplified FE-models

Three different types of simplified models are developed, for both cylindrical and tapered bearings. In all the models, the stiffness of the bearing is modeled, partly or entirely, with non-linear spring elements.

Model A is intended to give the correct stiffness and kinematics for radial and axial displacements as well as misalignment of the rings, but the deformation of the rings are not considered.

Model B should give the correct stiffness, but also the global deformation of the rings should be accurate. This means that the forces between rollers and rings are not modeled discrete; instead they are distributed over the raceways of the rings.

In Model C the force between rollers and rings is modeled discrete, i.e. the force at each roller-raceway contact and the detailed deformation of the ring is modelled. The force distribution inside the bearing and the deformation of the rings influence how the load is transferred from the bearing to the surrounding structure, see Section 4.4

3.1 Model A

Model A is intended to give the correct stiffness and kinematics, for both translations and misalignments. The deformation of the rings and the load distribution inside the bearing are not regarded. The coupling to the surrounding structure (typically shaft and bearing seat) is done via two *coupling nodes* in the centre of the bearing.

The stiffness of the bearing is modelled with spring elements. The springs are located at the same position as the rollers in the bearing, see Figure 3.1. This facilitates the calibration of the model with respect to the coupling between radial stiffness and the reactions moments for a misalignment. The springs are connected to the nodes at the centre of the model with kinematic couplings, see Figure 3.2. The kinematic couplings constrain the translation of the spring nodes to the translation of the nodes in centre of the model. This is comparable to having rigid rings in the model.

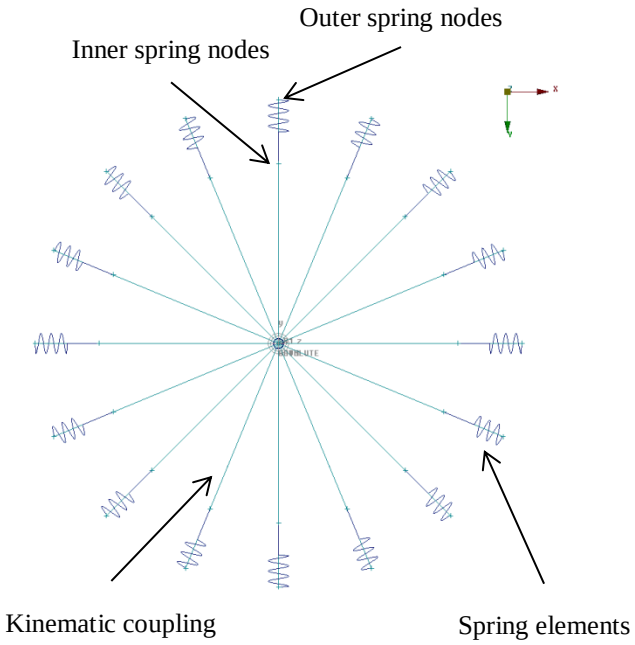

Figure 3.1 *Model A, the stiffness of the bearing is modelled with spring elements that are connected to coupling nodes in the centre.*

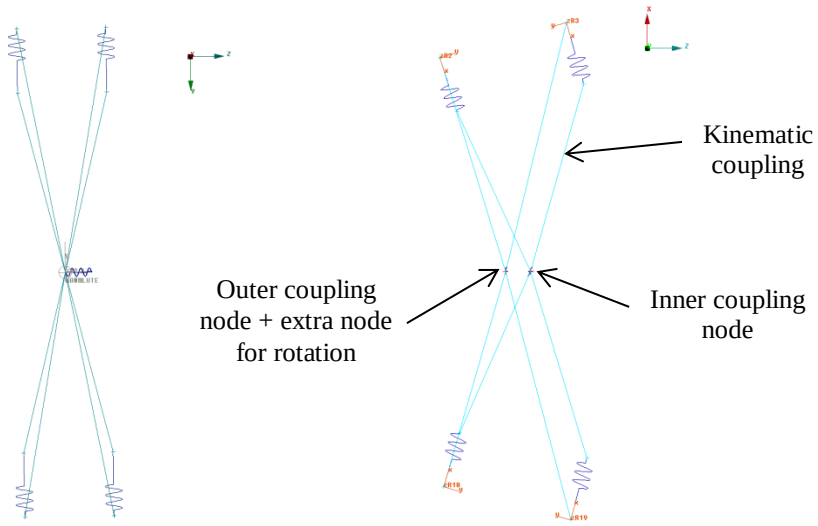

Figure 3.2 *Model A. Left: Cylindrical bearing. Right: Tapered bearing.*

In the centre of the bearing there are three nodes, the two *coupling nodes* and one node that is used to enable the bearing to rotate, see Figure 3.3. The inner coupling node is connected to the inner spring nodes with a kinematic coupling. There is also a kinematic coupling between the outer spring nodes and the extra node in the centre. The outer coupling node is not connected to the springs, but to the two other nodes in the centre. It is constrained to follow the motion of the extra node for all degrees of freedom except rotation around the z-axis. This enables the bearing to "rotate" around the z-axis (i.e. the axis parallel to the shaft).

For cylindrical bearings there is a spring that acts in the z-direction (axial direction in bearing) between the inner and outer coupling nodes, to model the axial stiffness. For tapered bearings the springs are orientated to be perpendicular to the raceways, hence

the axial stiffness is obtained in the correct direction in the bearing (negative z-direction in Figure 3.2).

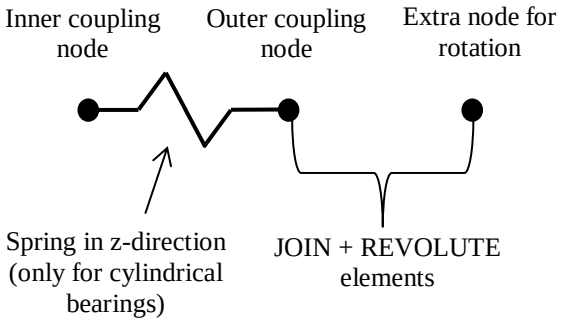

Figure 3.3 *Nodes and connection elements in the centre of the model. The inner coupling node is connected to the inner spring nodes with a kinematic coupling (not shown in figure). The extra node for rotation is connected to the outer spring nodes with a kinematic coupling (not shown in figure).*

3.2 Model B

Model B is formulated with the intention to give the correct stiffness and kinematics, but also the global deformation of the rings should be accurate, see Figure 3.4. The local deformation at each roller is not captured, but the deformation of the rings is smoother. This means that the forces between rollers and rings are not modelled at discrete positions but the forces are distributed over the raceways.

The structure of the models are the same for cylindrical and tapered bearings; the rollers are modelled with non-linear spring elements and the rings with cylindrical solid elements, see Figure 3.5. There is however a difference in how the load is transmitted between the rings and rollers for cylindrical and tapered bearings, especially when the bearing is subjected to an axial load, Section 3.2.2.

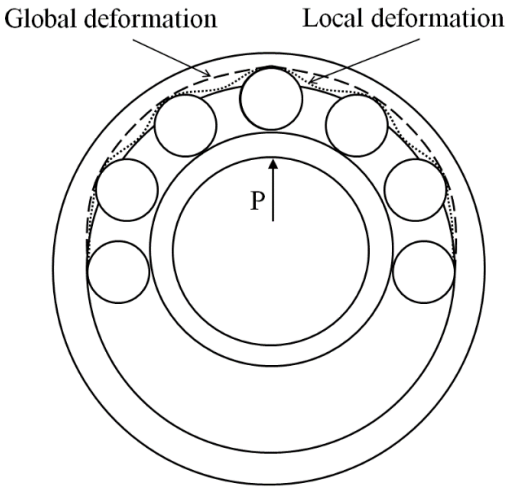

Figure 3.4 *Local deformation versus global deformation of the outer raceway.*

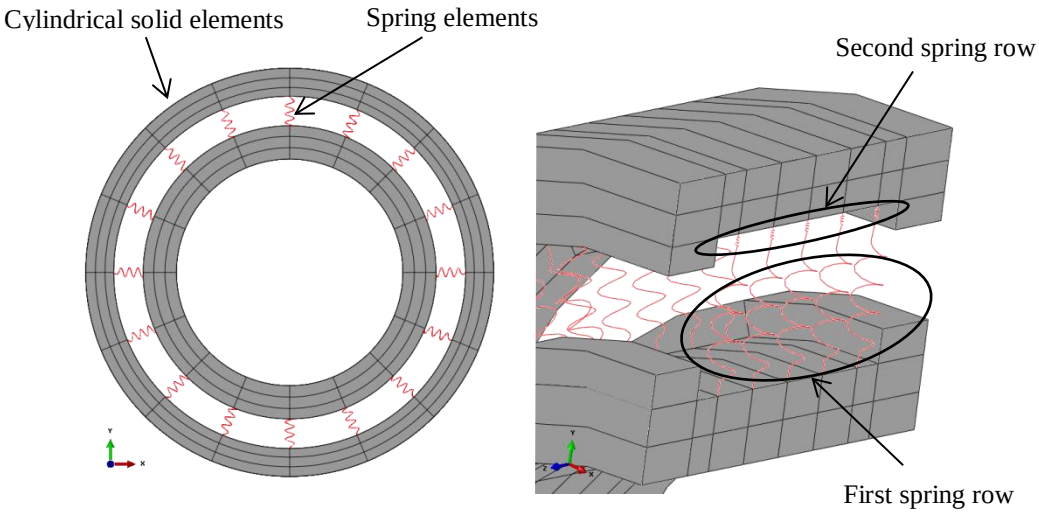

Figure 3.5 *a) Model B, each roller is modelled with a row of spring elements and rings with cylindrical solid elements. b) Spring elements between the rings to model the rollers in the bearing. Note that a cylindrical bearing is shown but tapered bearings are modelled in a similar manner.*

Each roller is modelled with a number of spring elements between the inner and outer ring, see Figure 3.5 b). Note that only a cylindrical bearing is shown but the rollers are modelled in a similar way for tapered bearings. Two rows of springs in series are used for each roller. The springs are connected to nodes belonging to the elements on the inner raceway, but a contact pair is used between the outer spring nodes and the outer raceway. This enables the inner ring to rotate with respect to the outer ring. The outer spring nodes and the nodes between the springs are constrained such that the springs remain perpendicular to the inner raceway.

3.2.1 Rings

The rings are modelled with second order cylindrical elements, see Figure 3.6. That is, 24-node cylindrical brick elements are used with quadratic basis functions in the radial plane and trigonometric basis functions in the circumferential direction (ABAQUS, 2013). Cylindrical elements is chosen because by having trigonometric basis functions in the circumferential direction, the surface inside and outside the bearing becomes cylindrical, even when a small number of elements is used in circumferential direction. When the bearing model is used in gearbox models, torsion of the shafts might cause the inner ring of the bearing to rotate slightly with respect to the outer ring. A smooth cylindrical surface then makes the contacts, used to enable the bearing to rotate, more stable. If the surfaces are not cylindrical the forces in the bearing and the deformation of the rings will vary with the position of the spring nodes. Also the contacts with shafts and housing become more stable with smooth inner and outer surfaces of the bearing.

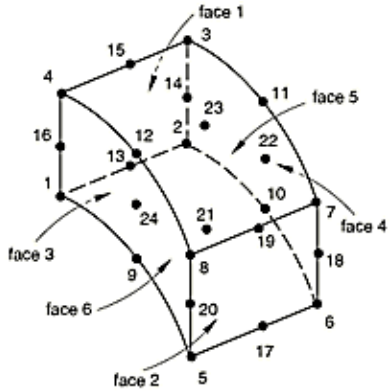

Figure 3.6 *24-node second order cylindrical element (CCL24R) (ABAQUS, 2013)*

As discussed in Section 2.2.1, the contacts between the rollers and rings are initially line contacts. When a load is applied a small contact area is formed. This could be achieved in the model by distributing the loads from the springs over an equally small area in the model, e.g. to the nodes adjacent to the spring nodes. But a force distributed over a small area leads to that the number of elements needs to be increased in this area in order to achieve mesh convergence.

The distribution of the forces could also be achieved by increasing the number of spring rows in the circumferential direction (i.e. using more spring rows than the actual number of rollers in the bearing). This will even out the forces on the rings, but also increase the number of elements since at least one element between each spring row is needed. In order to lower the number of elements needed to model the rings, the loads are instead "distributed" by using kinematic constraints that constrains the mid-nodes on the raceways. The displacement in the axial and radial direction of the mid-nodes on face 4 of IR and face 3 of OR is coupled to the displacement of the corner nodes (2, 3, 6, 7 and 1, 4, 5, 8 for IR and OR, respectively). One element is used between each spring row so this leads to a smoother deformation of the rings.

3.2.2 Roller-flange contact

The forces in the roller in cylindrical bearings due to an axial load (or misalignment of the bearing) act along the diagonal of the roller, see Figure 3.7. This introduces a moment that causes a misalignment of the roller that affects the stiffness of the bearing. To model this, rigid beam elements are connected to the flanges on the opposite side of the rings. In order to capture the rotation of the roller due to the axial load, and to get the force to enter the rings at the correct position, the beam elements are coupled to the displacement of the spring elements used for the radial stiffness. The axial play and axial stiffness is taken into account by using spring elements between the beams and the outer ring (not shown in the figure). The beams are connected to the rings in such a way that they are free to displace in the radial direction (as the springs are compressed). The outer ring is also free to rotate with respect to the beam elements.

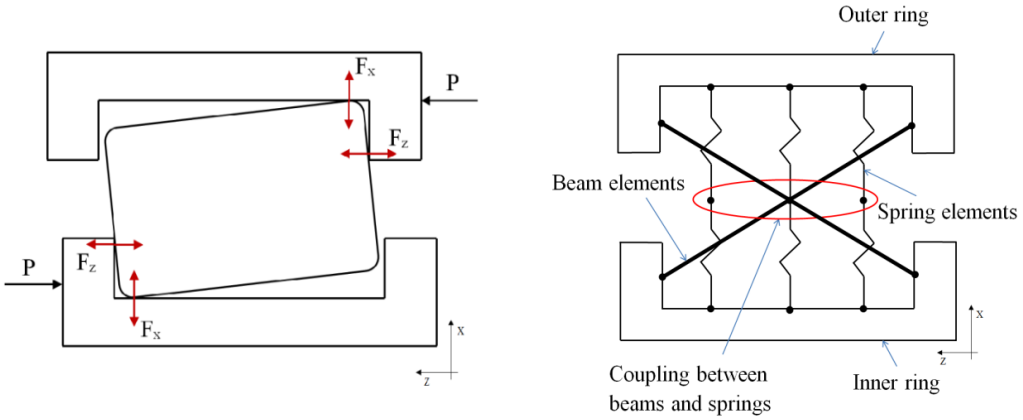

Figure 3.7 *a) Misalignment of roller in a cylindrical bearing subjected to an axial load, P b) The axial stiffness in the cylindrical bearing is modelled with beam elements between the flanges of the rings. Note that this is a simplified figure of the beam/spring arrangement.*

In tapered bearings, forces between the roller ends and the flanges of the inner ring occur for all load conditions, see Figure 3.8. Due to the angle of the raceways, a wedging effect will occur when the bearing is loaded in the axial direction. The spring nodes on the raceway are coupled to nodes on the left flange (in Figure 3.8) on the inner ring. This means that the spring loads will be distributed to the flange.

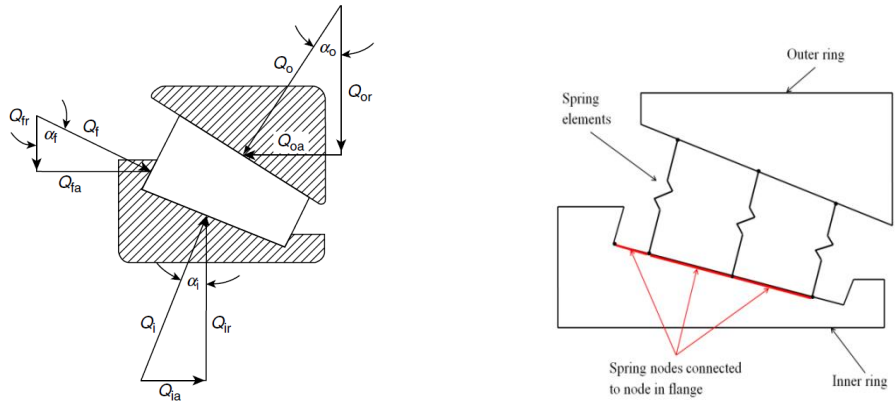

a) b)

Figure 3.8 *a) Forces between the roller and rings in a tapered bearing, when subjected to a combined axial and radial load (Harris, 2006) b) The spring nodes on the inner raceway are connected to the flange*

3.3 Model C

In Model C the forces between rollers and rings are modelled at discrete positions, i.e. the force in each roller is resolved. The rollers are modelled similar as in Model B, but two parallel rows of spring elements are used (each row consists of springs in series, as for Model B), see Figure 3.10. The contact area between rollers and rings is modelled with thin (in the circumferential direction) elements at each roller position, see Figure 3.9. In Section 2.2.1 the pressure distribution in the roller-raceway contact is shown. In the model the pressure is approximated as uniform in the circumferential direction over the contact area and replaced by the force resultants from the springs at the perimeter of the elements used to model the roller-raceway contact. If the elements have approximately the same width as the contact area formed the deformation of the rings should still be reasonably accurate.

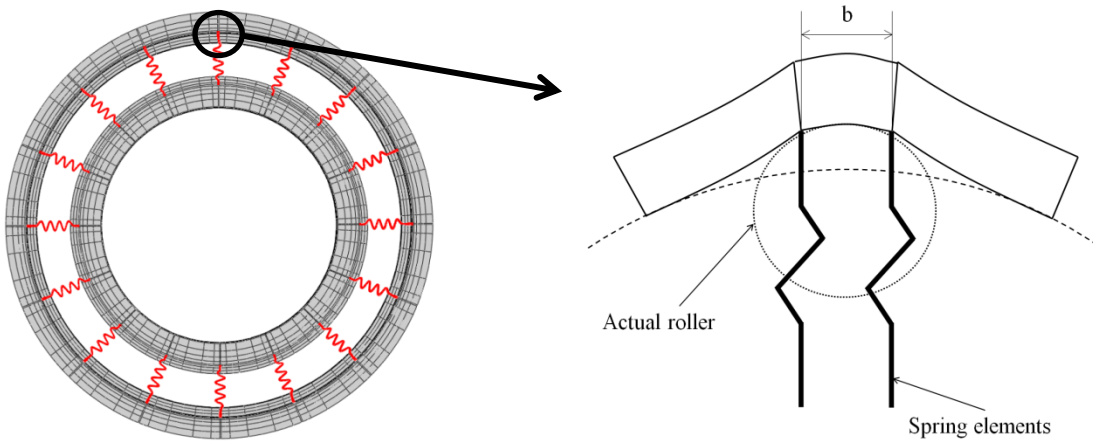

Figure 3.9 *Contact between outer raceway and roller. The spring elements are used to model the actual roller and the elements with width b in circumferential direction is used to model the contact area.*

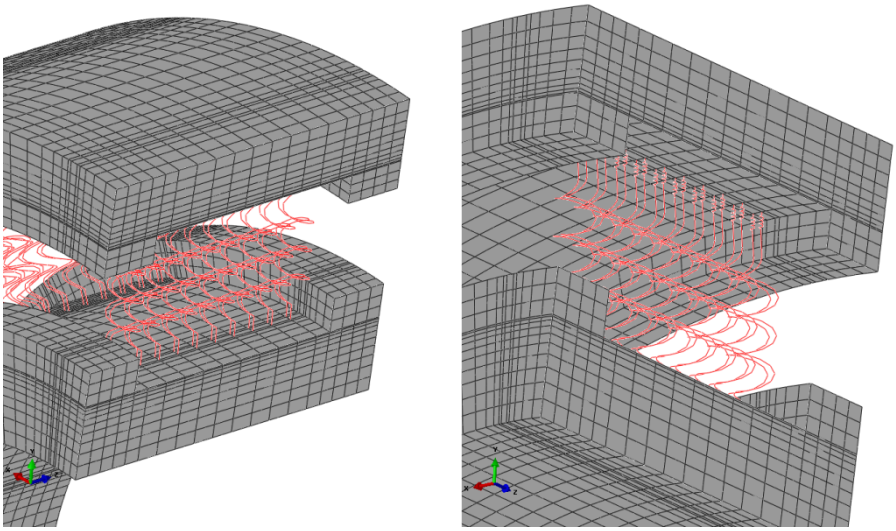

Figure 3.10 *Spring elements used to model the radial stiffness. Two parallel rows of springs are used; they are connected to an element with the width in the same order as the contact area formed between roller and raceway.*

This approach requires that the location of the spring nodes coincides with the elements used to model the contact area. Hence, the rings must not rotate with respect to each other. The spring nodes are constrained to coincide with the position of the nodes in the elements used to model the contact area.

The width of the contact area, b, varies with the roller load, see equation (2.3), but the magnitude is in the order of 10^{-1} mm for roller loads under 5kN/mm. The deformation inside the bearing, at the roller contact, is smoothened out through the thickness of the rings, see Section 4.4. Hence, since the model is not used to analyse the bearing, but the surrounding structure, the exact width of the contact area should not be critical.

For this model the bending of the roller due to misalignment may have some effect since the detailed deformation of the rings is of interest. But the ratio between the diameter and length of the roller may be considered small for most of the roller bearings to be modelled. Hence, this effect can probably be neglected, but this needs to be verified.

The axial stiffness for cylindrical bearings is modelled in the same way as for Model B, i.e. with beam elements between the flanges of the rings that are coupled to the spring rows (see Figure 3.7). One arrangement of beam element is used for each spring row, i.e. two arrangements of beam elements for each roller. The load distribution to the flange on the inner ring for tapered bearing is done in the same way as for Model B, see Figure 3.8.

3.4 Spring stiffness

The stiffness of the springs is non-linear to account for the non-linear behaviour of the roller-raceway contact, see Section 2.2. Since the rollers in a bearing can only take a compressive load, the force in tension should be zero. But to enhance the stability of the models and the initial conditions, the springs have a small stiffness also in tension. The relation between the force and displacement for the springs can be seen in Figure 3.11. The radial play of the bearing is also included in the spring stiffness. The rollers have a convex profile to avoid stress concentration at the roller ends, Harris (1991). This is included in the models by adjusting the radial play, i.e. the offset in the spring stiffness, depending on the axial position of the springs in each spring row. The springs have a small stiffness also for the radial play to enhance the stability of the models.

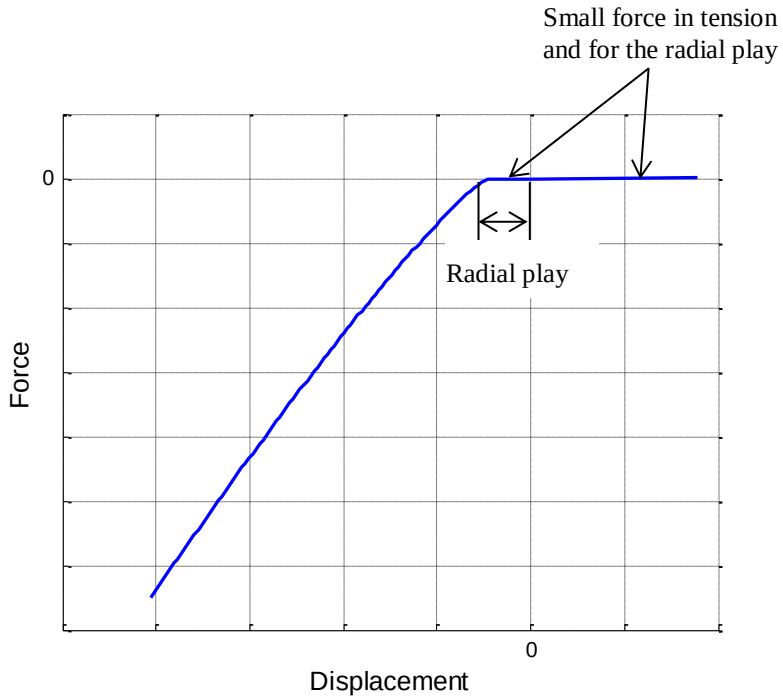

Figure 3.11 *Sketch of force-displacement relation for the non-linear spring elements used to model the rollers.*

The spring stiffness is based on the load-deflection relations in Section 2.2.2. Those relations are valid for two remote stress free points in the rings and the rollers; hence especially for Model B and C the relations need to be adjusted. The springs in Model A is used to model the stiffness of both the rollers and the rings so the analytical expressions should be fairly accurate.

In Model B the rings are modelled with deformable solid elements so the stiffness of the springs should only include the deformation of the rollers. Hence, the springs should be a bit stiffer than what is described by the analytical expressions. The force from the springs is not modelled at discrete location at the rings, but distributed over the raceway, this also affects the spring stiffness required in order to get the correct overall stiffness in the bearing. Since the deformation of the rings is constrained to

obtain the load distribution, some of the deformation of the rings needs to be included in the springs by lowering the stiffness.

Also in Model C the rings are modelled with deformable solid elements but the forces from the springs is modelled at discrete locations. This yields a higher required spring stiffness than for Model B since the deformation of the rings should be fairly accurate. The spring stiffness in the models are calibrated against reference results from complete FE-models, see Appendix C.

4 Evaluation of models

The evaluation of the models was performed based on the geometry of SKF XX cylindrical bearing, see Appendix B for input data. The mesh convergence for the models of type B and C was studied as well as the stability of the Model B when subjected to a rotation around the z-axis (parallel to shaft). The effects on the load distribution to the surrounding structure for Model B and C were studied by simulating a bearing that is built into a disc representing the bearing housing.

The computational cost for one simple load case is presented in Table 4.1. The outer ring was fixed and a radial force was applied to the inner ring. From a computational cost aspect the main difference between the models is the number of degrees of freedom. It can be seen that the number of iterations is significantly lower for Model A than for the other two. Also the CPU time is lower. The number of iterations for Model B and C is similar, but the CPU time is lower for Model B.

Table 4.1 *Computational cost for one simple load case for the different models for cylindrical bearing. A radial force was applied on the inner ring and the outer surface of the outer ring was fixed.*

Model	Number of elements	Iterations	CPU Time [sec]
A	35	2	0.13
B	256	14	35
C	20128	15	1098

4.1 Model B

4.1.1 Mesh convergence

The mesh convergence was studied for the simple load case defined by fixing the outside of the outer ring and applying a radial force to the inner ring. The radial displacement of the centre of the inner ring was used to measure the convergence. The same number of elements was used for the inner and outer ring. Different element types (first and second order cylindrical elements and second order brick elements) were studied, for comparison. The element types were tested with and without load distribution on the raceways.

The number of elements in the rings and the number of springs per roller were both increased uniformly in all directions (axial, radial and circumferential). The resulting convergence for the different element types, with and without load distribution can be seen in Figure 4.1. It can be observed that the model converges faster when the load is distributed over the raceway, and that the convergence is almost identical for the different element types when load distribution is used.

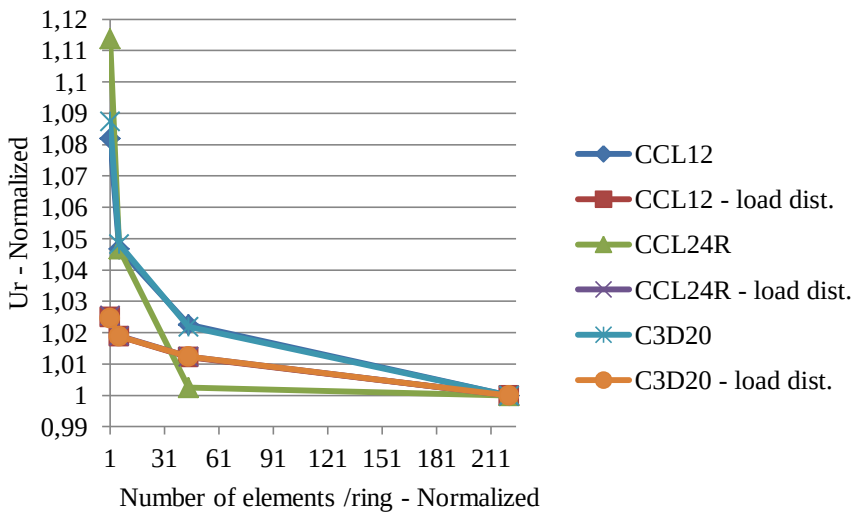

Figure 4.1 *Convergence for the first and second order cylindrical elements (CCL12 and CCL24R) and second order brick elements (C3D20), with and without load distribution (- load dist.). Note that the values have been normalized.*

The difference in radial displacement between the coarsest and the finest mesh without load distribution is about 8-12%. When load distribution is used the difference is around 2.5%. It may also be noted that with CCL24R elements convergence is reached for the third mesh.

4.1.2 Rotation stability

When the model is used in gearbox models, torsion of the shafts might cause the inner ring of the bearing to rotate slightly with respect to the outer ring. Since the spring elements are attached to the inner ring, they will rotate with it. The rotation of the inner ring will therefore affect the results (in particular the stiffness of the bearing) for two reasons. The first reason is that the load distribution among the spring rows (i.e. rollers) will alter as the position of the rollers with respect to the direction of the force change. The second reason is that the position of the spring nodes on the elements on the outer raceway change. Initially they are lined up with the corner nodes on the outer elements.

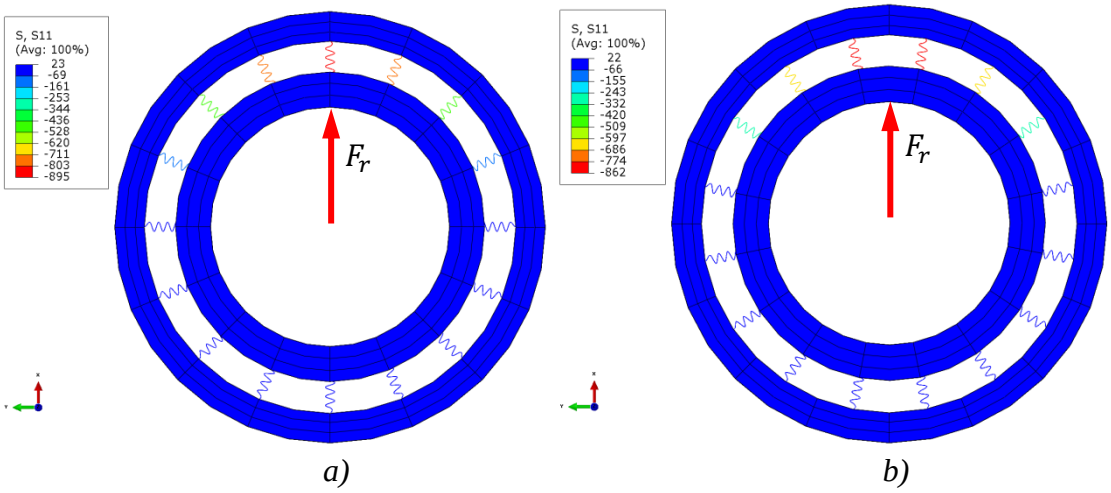

Figure 4.2 *a) Initial position of the springs and the direction of the radial force. Also the load distribution in the spring elements can be seen. b) Load distribution in the spring elements when the inner ring is rotated an angle corresponding to half an element in the circumferential direction.*

Mesh 1, see previous Section, is used to test the stability of the model. Initially the rings and the spring elements where lined up according to Figure 4.2 a). A radial load, F_r, was applied and then the rings was rotated with respect to each other.

Figure 4.2 b) shows how the load is distributed over the rollers (spring elements) when the inner ring is rotated an angle corresponding to half an element in the circumferential direction. It is shown that the load is distributed over more spring rows compared to the initial position. Hence, the radial stiffness is increased and the radial displacement is decreased. Figure 4.3 a) shows the variation of the radial displacement (of the centre of the inner ring) for the rotation over one element, in the circumferential direction, on the outer raceway. It can be seen that the displacement varies with the position of the spring nodes on the elements on the outer ring. When IR is rotated the distribution of the force in the roller will change, so this curve describes the variation due the spring node position on the outer ring and the load distribution among spring rows. When OR is rotated only the position of the spring nodes on the outer ring change, not the load distribution among the spring rows.

Figure 4.3 b) shows the variation in the radial displacement when the rings are rotated 360°. It can be seen that the change in displacement is repeating for each element circumferentially and that it does not grow or decrease, this indicates that the model is stable. The maximum variation in radial displacement compared to the initial solution is about -0.4%. If the load is not distributed over the elements, the difference in radial displacement should become larger due to the change in number of rollers in contact. Also a bearing with a lower number of rollers should give a larger variation.

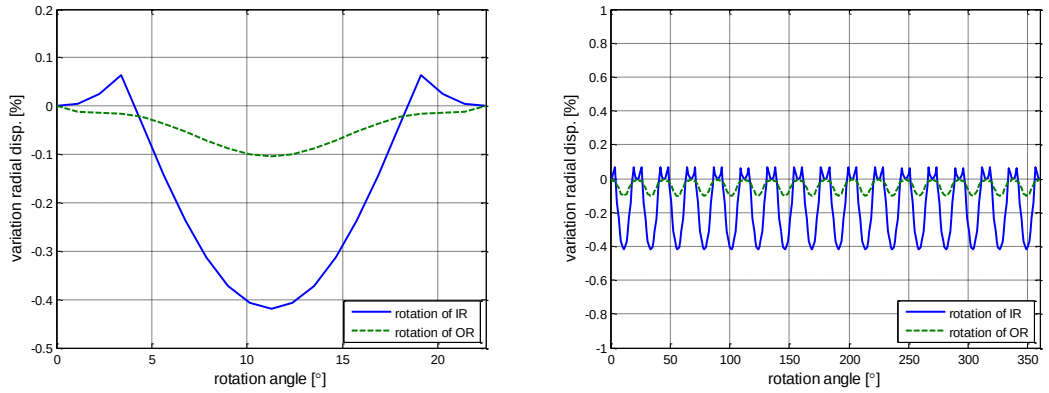

a) *b)*

Figure 4.3 *Radial displacement versus rotation of the rings. One element in the circumferential direction is used between each roller position on the rings. a) Rotation over one element in the circumferential direction. b) 360° Rotation of the inner ring.*

Figure 4.4 shows how the axial displacement varies if the bearing is rotated when subjected to a pure axial load. The variation is independent of which ring that is rotated, as expected. For this case the load distribution among the rollers does not change when the bearing is rotated. But the obtained variation is due to the position of the end nodes, on the beams used to model the roller ends, with respect to the elements inside the flanges on the outer ring. The load is distributed over these elements as well, but small fluctuations in the axial displacement can be seen. Also for this case the model seems to be stable when subjected to a large rotation. The maximum variation of the axial displacement with respect to the result for the initial position of the rings, is about -0.27% which can be regarded as negligibly small.

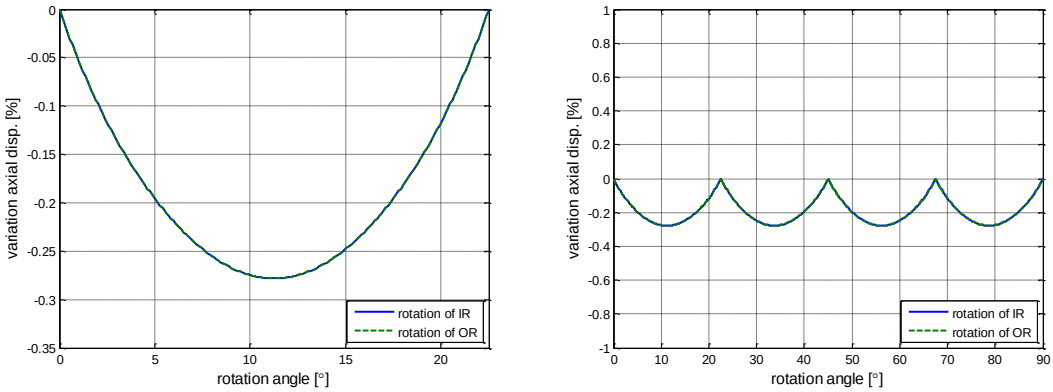

a) *b)*

Figure 4.4 *Variation in axial displacement versus rotation of the rings. One element in the circumferential direction is used between each roller position on the rings. a) Rotation over one element in the circumferential direction. b) 360° Rotation of the inner ring.*

4.2 Model C

4.2.1 Mesh convergence

The mesh convergence for Model C was studied by increasing the number of elements uniformly in all direction, including the number of spring elements in each row. The meshes are shown in Figure 4.5. The outside of the outer ring was fixed and a radial force was applied to the inner ring. The radial displacement of the centre of the inner ring was used to measure the convergence. The same number of elements was used for the inner and outer ring. The results can be seen in Table 4.2. The change in radial displacement is small, the difference between the coarsest and finest mesh is about 0.2%.

Table 4.2 *Mesh convergence for Model C.*

Number of elements	Radial displacement [mm]	Iterations	CPU Time [sec]
20128	0,03894	15	1098
79168	0,03888	15	11500
332128	0,03885	16	174185

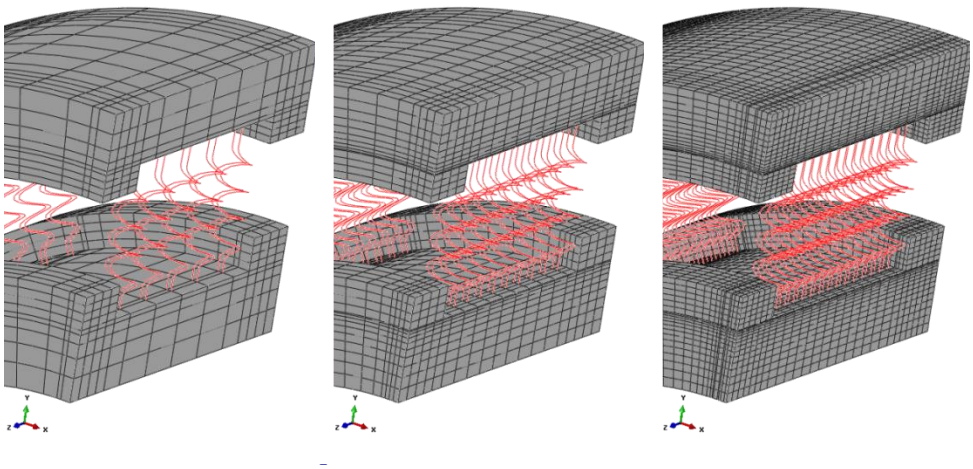

Figure 4.5 *Meshes used in convergence study for Model C. Left to right: Coarse to fine.*

4.3 Forces and moments

The spring stiffness in the models for cylindrical bearings was calibrated against results from a complete FE-model of the bearing. The complete model is regarded as a guideline for the simplified models. The resulting expressions for the stiffness are presented in Appendix C.

Figure 4.6 shows the force versus displacement for the reference model, the simplified models and analytical solutions from Harris (1991) and Houpert (1997) (see Appendix A for equations). The simplified models and the reference model give similar behaviour of the bearing after the calibration of the spring stiffness. Harris approach gives a bit stiffer response for the bearing, especially for small displacements; this might be due to that the profile of the rollers is not included in the equations. Houpert's approach gives instead a weaker response of the bearing with a higher initial stiffness. The weaker response could be related to his expression for the load-deflection relation for the roller-raceway contact, see Section 2.2.2.

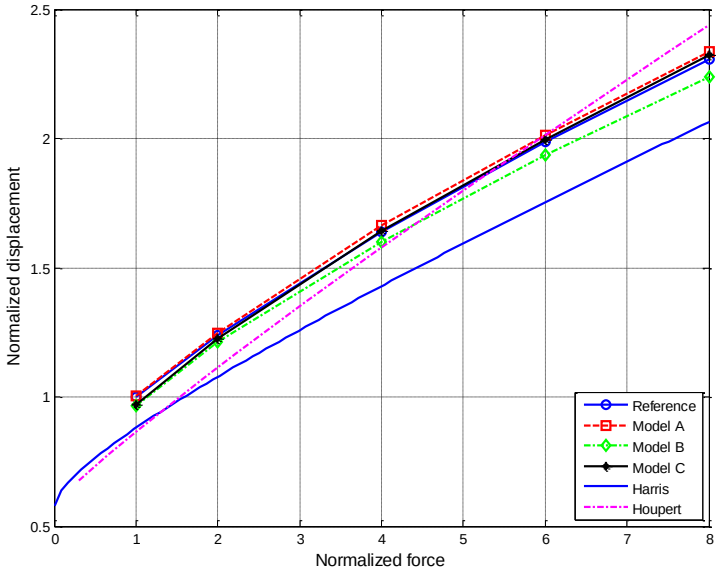

Figure 4.6 *Force versus displacement for the cylindrical bearing.*

Figure 4.7 shows the error for the simplified models against the reference for the computed displacement versus the normalized applied force. The error is approximately constant for Model A and B, this indicates that the non-linearity of the stiffness in the models is approximated accurate. For model C the error is larger for smaller forces. This indicates that the expression for the load-deflection relation in the spring elements should be adjusted and that the initial stiffness of bearing is too small.

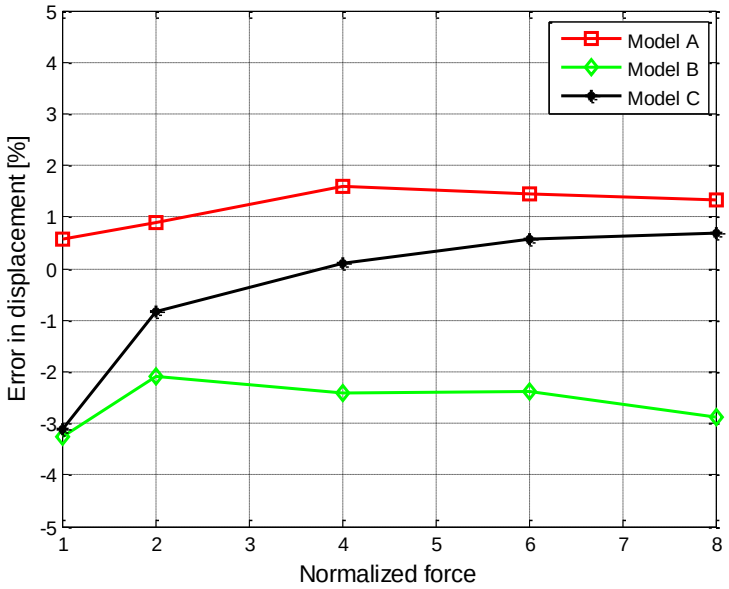

Figure 4.7 *Error in displacement versus normalized force for cylindrical bearing.*

Figure 4.8 shows the moment versus misalignment for the bearing models. Also for these the agreement between the reference model and the simplified bearing models are satisfactory after calibration of the spring stiffness. Houpert's equations give a similar behaviour of the bearing, but the response is a bit stiffer for larger misalignments.

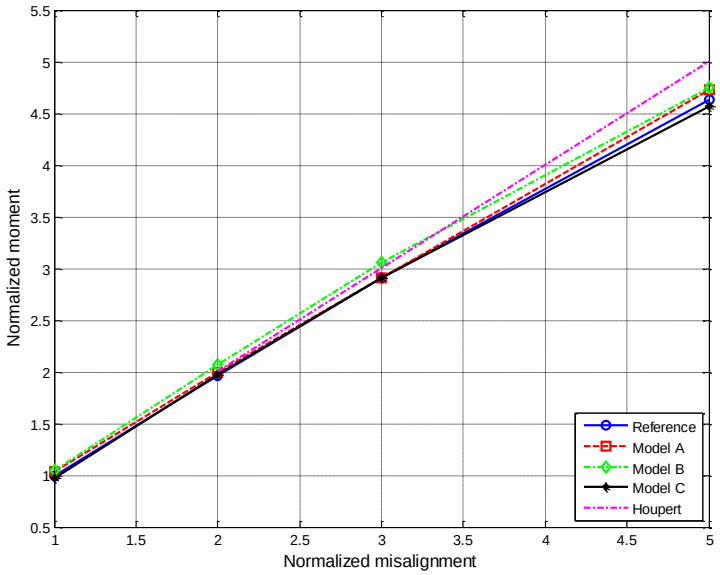

Figure 4.8 *Moment versus misalignment for cylindrical bearing.*

Figure 4.9 shows the error for the simplified models against the reference for the reaction moment versus normalized misalignment. The error seems to be larger for small misalignments. It could be mentioned that even though the largest error in percentage is between 3-5% for the models, the difference in absolute values could be considered small.

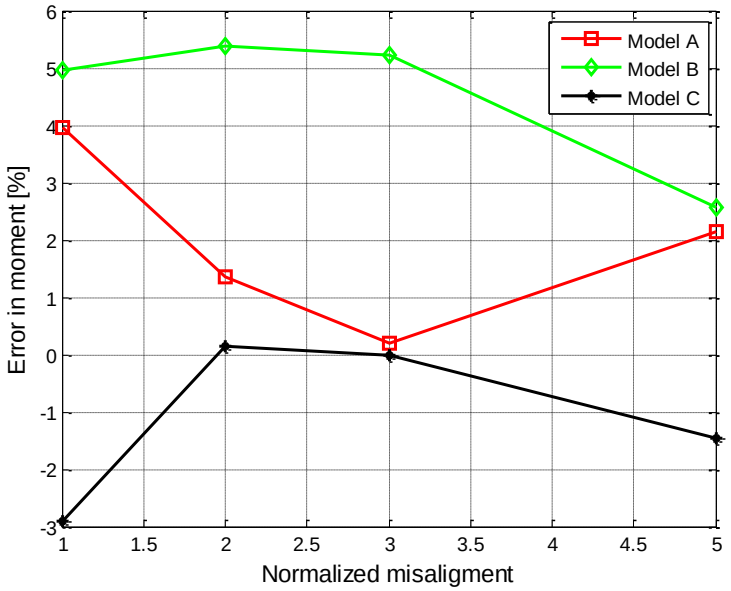

Figure 4.9 *Error in reaction moment versus normalized misalignment for cylindrical bearing.*

4.4 Force distribution in the surrounding structure

The bearing models are not intended to be used to analyse bearings, but to introduce forces to the surrounding structure in the gearbox. Hence, it is of interest to analyse what effects the simplifications made have on the load distribution in the surrounding structure. In Model B the roller forces are distributed over the raceways, while in Model C the forces between the rollers and the rings are modelled at discrete locations. This affects how the force enters the bearing housing. For Model B the deformation of the rings is smoother, while Model C the local deformation at each roller-raceway contact is captured. Note that in Model A the coupling to the surrounding structure is done via two nodes in the centre of the model, hence it does not make sense to evaluate the force distribution for this model.

The two models are simulated in an assembly with two discs, representing a shaft and the bearing seat. The housing is made of aluminium and the shaft is made of steel. The plate with bearing Model B is shown in Figure 4.10.

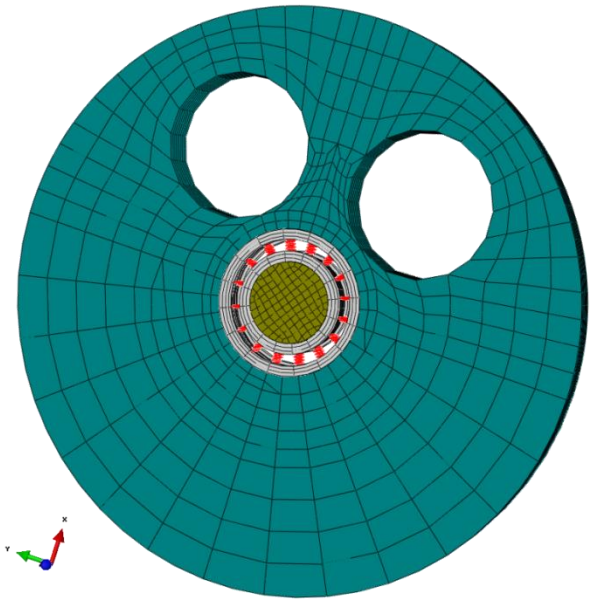

Figure 4.10 *Cylindrical roller bearings built in a structure consisting of two discs, representing a shaft and bearing seat.*

The meshes for the models can be seen in Figure 4.11. Note that due to the structure of the models, with the load distribution for Model B etc., the meshes for the bearings are quite different. Model B is intended to use with a small number of elements in the circumferential direction. The width, in circumferential direction, of the elements used to model the roller-raceway contact in Model C is set to 0.25mm which corresponds to a roller load of approximately 0.5kN/mm according to equation (2.3).

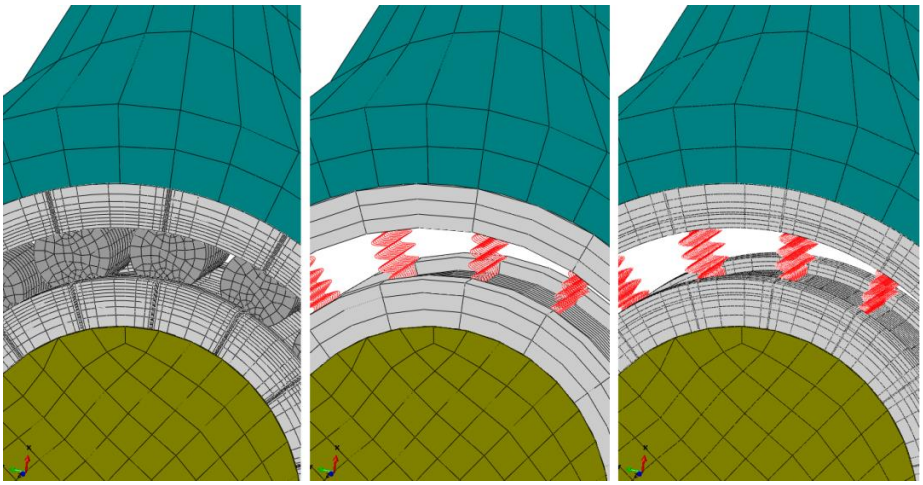

Figure 4.11 *Models used in the simulations. Left: Reference Middle: Model B Right: Model C.*

A radial load is applied to the shaft and the outer surface of the outer plate is fixed. Figure 4.12 shows the stress distribution in the outer plate for the two simplified models and for a complete FE-model of the bearing. The stress distribution in the plate is similar for all the bearing models. Close to the bearing seat some difference

between Model B and C can be seen, due to the difference in the distribution of the roller loads. Figure 4.13 shows the stress distribution in the contact between the bearings and the outer disc (cut in the middle of the disc in). The force enters the disc a discrete locations for Model C and the reference model, while for Model B the force is smoothen out and distributed over a larger area of the bearing seat. This indicates that if the stress in the area close to the bearing is of interest, Model B may be not appropriate to use, but the differences is small. However, if the detailed deformation of the bearing seat is of interest then Model B is not sufficient but the more discrete modelling of the forces in Model C is needed.

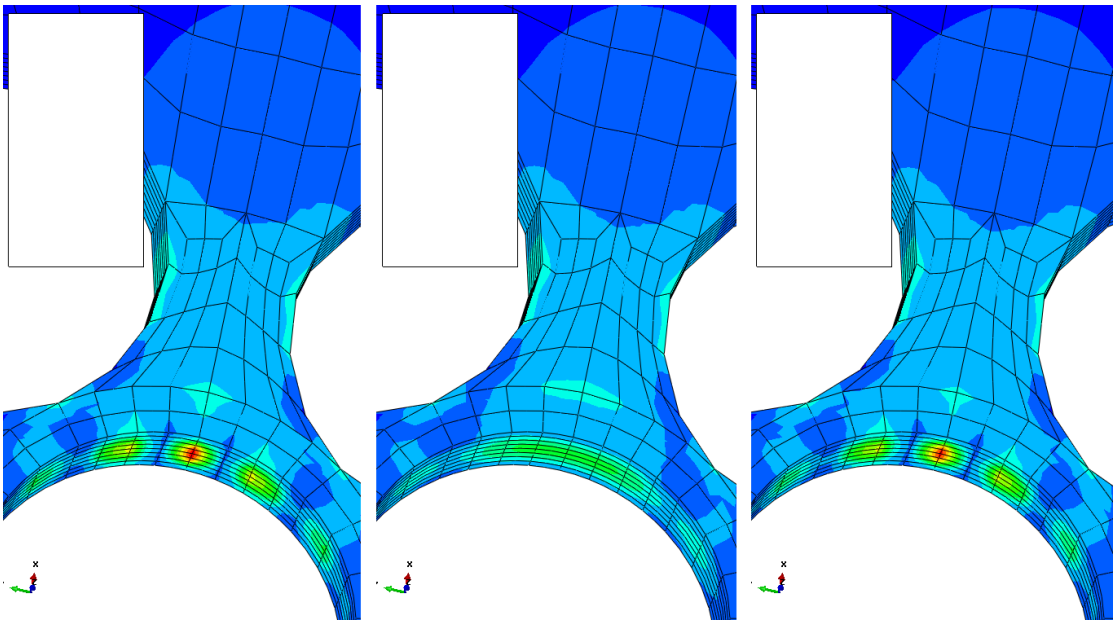

Figure 4.12 *Stress distribution in the outer disc, representing bearing seat. Left: Reference Middle: Model B Right: Model C. Note that the same scale is used for the stress in all the figures.*

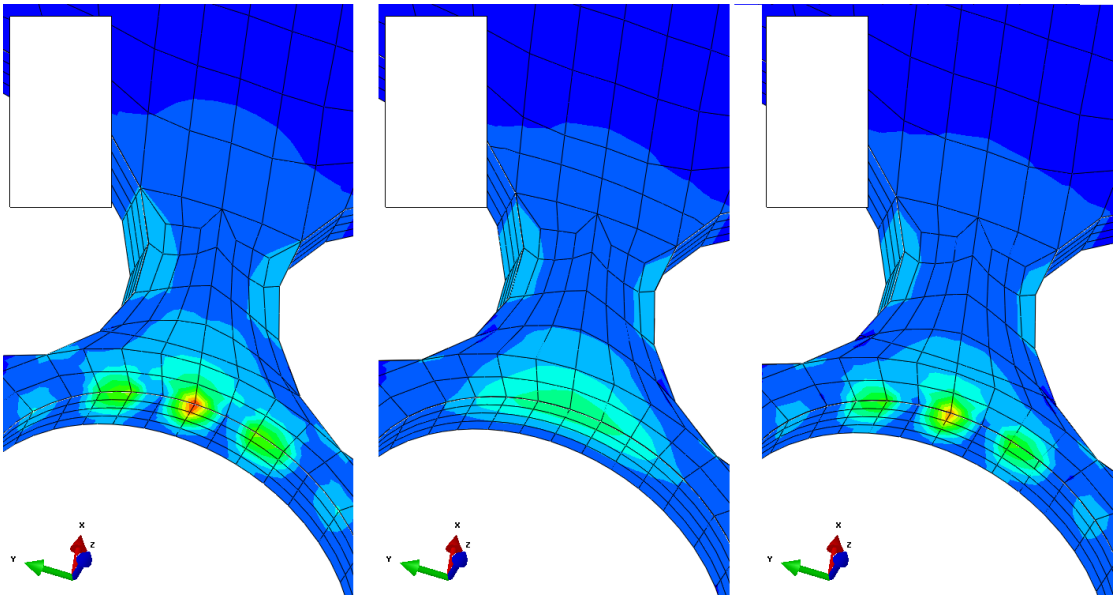

Figure 4.13 *Stress distribution in the outer disc, representing bearing seat, cut in the middle of the disc. Left: Reference Middle: Model B Right: Model C. Note that the same scale is used for the stress in all the figures.*

5 Conclusions and discussion

Figure 4.6 and Figure 4.8 indicates that the behaviour of the simplified models for cylindrical bearings, in the radial direction and for misalignment, is similar to that of the reference model. However, more load cases with different boundary conditions, e.g. the bearing built in to different structures, should be evaluated. Also bearings with different geometry and number of rollers should be evaluated.

The relation between force and displacement is captured more correct than the relation between misalignment and reaction moment, see Figure 4.7 and Figure 4.9. This indicates that the axial position of the spring elements that are used to model the rollers should be investigated further. The springs in Model B and C is connected to elements on the inner ring and constrained to be perpendicular to the inner raceway. If the inner ring is misaligned the springs follows with the rotation. Due to the geometry of the raceways the affect from constraining the springs to the outer ring instead should be investigated.

Figure 4.6 and Figure 4.8 also shows that the analytical solutions from Harris and Houpert give a fairly good approximation of the forces and moments in cylindrical bearings, with Houpert's approach being a bit closer to the reference results.

Model A seems to give satisfactory results for decoupled forces and moments. However, the coupling between an axial displacement and the moments and radial forces is not included in the model for cylindrical bearings.

Figure 4.12 and Figure 4.13 indicates that the stress distribution in the surrounding structure is similar for the reference model and Model B only a short distance from the model, approximately twice the roller diameter. The deformation of the bearing seat is however smoother for Model B and the detailed deformation at each roller is not captured, if this is of interest then Model B is not sufficient to use.

In Section 4.1.2 it was shown the radial and axial displacement in the bearing is stable when the rings are rotated with respect to each other. The variation due to the contact between the spring nodes and the outer raceway (mesh dependence) was small. It was also shown that the load distribution among the spring rows varies with respect to the direction of the force as the inner ring is rotated; leading to a variation in the radial displacement, but the variation was small. The deformation of the rings is constrained to be smooth so this variation might actually be too small compared to an actual bearing.

Figure 4.12 and Figure 4.13 shows that the stress and load distribution on the structure surrounding the bearing are similar for the reference model and Model C. This indicates that the deformation of the rings and the load distribution in the bearing is similar for the two models. The force distribution is modelled as uniform in circumferential direction over the contact area for the roller-raceway contact in Model C, which is an approximation. The effects from modelling the force distribution more accurate, e.g. according to a Hertz-like pressure distribution could be investigated. However, the comparison with the reference model shows that the approximation used seems to give sufficient accuracy for the deformation and load distribution outside the bearing.

6 Recommendations and future work

- Model C is intended to capture the detailed deformation of the rings in the bearing. However, bending of the rollers is not included. The rollers are quite stiff in this direction due to the diameter/length ratio being small but the effects from modelling the roller as flexible, e.g. using beam elements, should be investigated further.

- The spring stiffness for the tapered models should be approximately the same as for the cylindrical bearings. But this needs to be verified.

- The spring elements used to model the stiffness in the axial direction for cylindrical bearings needs to be calibrated against reference results.

- The bearing models can be generated from a limited number of parameters describing the bearing geometry but to facilitate the use of the models, a graphical user interface should be implemented

7 References

ABAQUS (2013): *ABAQUS Documentation*, Dassault Systems, Providence, RI, USA

Brändlein, J., Eschmann, P., Hasbargen, L., Weigand, K. (1999) *Ball and Roller Bearings: Theory, Design and Application,* Third Edition, Wiley, Sussex, {England}

Harris, T. A. (1991): *Rolling bearing analysis*. Wiley, New York, {USA}, {1991}, 3rd edition, 1013 pp.

Harris, T. A., Kotzalas, M. N. (2006): *Essential Concepts of Bearing Technology*, Fifth Edition, ISBN: 978-0-8493-7183-7

Harris, T. A., Kotzalas, M. N. (2006): *Advanced Concepts of Bearing Technology*. CRC Press, {2006}, ISBN: 978-0-8493-7182-0

Houpert, L. (1997): A Uniform Analytical Approach for Ball and Roller Bearings Calculations. *Journal of Tribology,* Vol. 119, {October} 1997, pp. 851-858.

Palmgren, A. (1959): *Ball and Roller Bearing Engineering*. 3rd ed., Burbank, {Philadelphia}, {1959}

A Analytical approach for bearing race loads and moments

A.1 Cylindrical bearing subjected to pure radial load

Harris (1991) derives analytical expressions for determining of the total stiffness of a roller bearings subjected to a pure radial load. By studying static equilibrium, he shows that the radial force, F_r, on the bearing is related to the radial displacement, δ_r, as:

$$F_r = ZK_n(\delta_r - 0.5P_d)^n J_r(\epsilon) \tag{A.1}$$

Where J_r is the so called Sjövall integral:

$$J_r(\epsilon) = \frac{1}{2\pi}\int_{-\psi_l}^{+\psi_l}\left[1 - \frac{1}{2\epsilon}(1-\cos\psi)\right]^n \cos\psi \, \mathrm{d}\psi \tag{A.2}$$

Where ψ_l is the angle of load zone extent:

$$\psi_l = \cos^{-1}\left(\frac{P_d}{2\delta_r}\right) \tag{A.3}$$

And ϵ is the relation between the diametral play, P_d, in bearing and the radial displacement according to:

$$\epsilon = \frac{1}{2}\left(1 - \frac{P_d}{2\delta_r}\right) \tag{A.4}$$

Equation (A.1)– (A.4) can be solved, using iterations, for the radial displacement for a given radial force, or vice versa.

A.2 General loading of tapered and cylindrical bearings

Equations for calculating the bearing inner race loads and moments, based on the kinematic relation in Section 2.1, see also Houpert (1997).

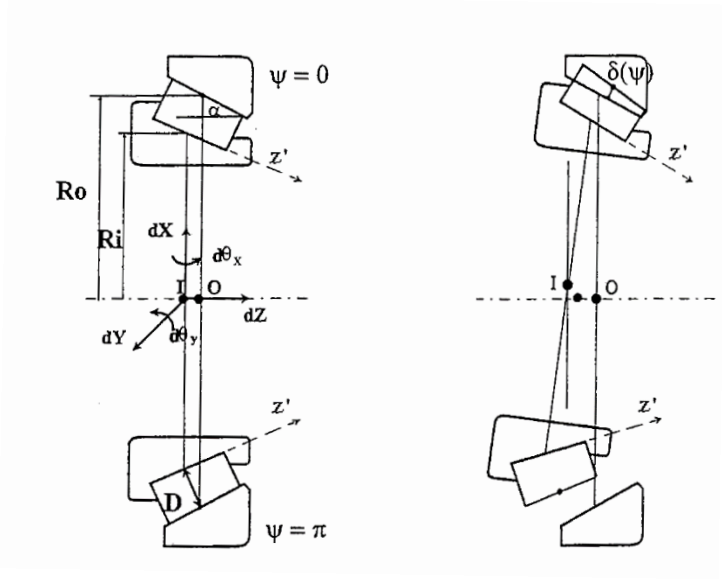

Figure A.1 *Displacement of the centre of the inner ring (point I) with respect to the centre of the outer ring (point O) (Houpert ,1997). a) Position of the rings when the bearing is undeformed. b) Inner ring displaced with respect to the outer ring.*

A.2.1 Bearing inner race forces

Equivalent displacements of the centre of the inner roller-raceway contact:

$$D_x = d_x + d\theta_y Ri \tan\alpha \tag{A.5}$$

$$D_y = d_y - d\theta_x Ri \tan\alpha \tag{A.6}$$

$$D_r = \sqrt{D_x^2 + D_y^2} \tag{A.7}$$

Summation of the roller loads, by integrating over ψ for the number of rollers in contact, gives:

$$F_z = -K(D_r \cos\alpha)^n \sin\alpha \frac{Z}{2\pi} \int_{-arcos(-A)}^{arcos(-A)} (\cos\psi' + A)^n d\psi' \tag{A.8}$$

$$F_r = -K(D_r \cos\alpha)^n \cos\alpha \frac{Z}{2\pi} \int_{-arcos(-A)}^{arcos(-A)} (\cos\psi' + A)^n \cos\psi' \, d\psi' \tag{A.9}$$

$$F_x = F_r \cos \psi_r \tag{A.10}$$

$$F_y = F_r \sin \psi_r \tag{A.11}$$

and ψ_r is the angle for the position of the roller where the maximum roller load will occur:

$$\psi_r = \tan^{-1} \frac{D_y}{D_x} \qquad \text{if } D_x > 0 \tag{A.12}$$

$$\psi_r = \tan^{-1} \frac{D_y}{D_x} + \pi \quad \text{if } D_x < 0 \tag{A.13}$$

and ψ' is:

$$\psi' = \psi - \psi_r \tag{A.14}$$

A is a parameter that combines the displacements in the axial and radial direction, that is used to determine the angle for the number of rollers in contact:

$$A = \frac{-dz \sin \alpha}{D_r \cos \alpha} \tag{A.15}$$

A.2.2 Bearing inner ring moments

The radial loads and a misalignment of the inner ring with respect to the outer ring give rise to moments in the centre of the inner ring. If the contact angle between the rollers and raceway is assumed to be constant, the moment due to the radial loads and misalignments are:

$$M_{x,I} = -Ri \tan \alpha \, F_y + \Delta M_x \tag{A.16}$$

$$M_{y,I} = Ri \tan \alpha \, F_x + \Delta M_y \tag{A.17}$$

The additional tilting moment due to the misalignment, ΔM_i, can be approximated by, assuming that the roller-raceway deformation is small:

$$\Delta M_x = \frac{0.33}{12} K L^2 \frac{Z}{2\pi} (E \, d\theta_x + F \, d\theta_y) \tag{A.18}$$

$$\Delta M_y = \frac{0.33}{12} K L^2 \frac{Z}{2\pi} (F \, d\theta_x + G \, d\theta_y) \tag{A.19}$$

Where E, F and G are integrals over the number of rollers in contact that can be approximated with the analytical expressions in Table 8.1.

Table A.1 *Analytical expressions for E, F and G (Houpert, 1997)*

For $A \leq 1$	For $A > 1$
$E = arcos(-A) + A\sqrt{1 - A^2}\cos(2\psi_r)$	$E = \pi$
$F = 2A\sqrt{1 - A^2}\cos\psi_r \sin\psi_r$	$F = 0$
$G = arcos(-A) - A\sqrt{1 - A^2}\cos(2\psi_r)$	$G = \pi$

B Appendix Volvo GTT

C Appendix Volvo GTT

D Appendix Volvo GTT